Charge-Transfer Character in a Covalent Diketopyrrolopyrrole Dimer: Implications for Singlet Fission

Catherine M. Mauck, Youn Jue Bae, Michelle Chen, Natalia Powers-Riggs, Yi-Lin Wu, and Michael R. Wasielewski*[a]

Diketopyrrolopyrrole (DPP) is a strongly absorbing, photostable chromophore that can undergo singlet fission (SF), a photophysical process that promises to significantly enhance solar-cell performance. In the solid state, DPP packs in a herringbone arrangement that maximizes intermolecular donor–acceptor interactions, suggesting that charge-transfer (CT) states play a role in DPP SF. In order to characterize intermolecular DPP CT states in molecular assemblies, we have synthesized a covalent DPP dimer bridged by a xanthene linker, which places two thiophene-substituted DPPs (TDPPs) in a cofacial arrangement that mimics chromophore p–p stacking in the thin film. After photoexcitation in polar solvents, symmetry-breaking charge separation forms the fully charge separated TDPP^{+}C–TDPP$^{@}$C ion-pair state. In nonpolar solvents, charge separation is incomplete leading to the TDPP^{d+}–TDPP$^{d@}$ CT state, which is in pseudoequilibrium with the relaxed S_1S_0 state observed by transient absorption and emission spectroscopy. This study highlights the importance of intramolecular coupling as well as the importance of entropy to promoting SF in chromophore dimers for which SF is endo- or isoergic.

1. Introduction

3,6-Diaryl-1,4-diketopyrrolo[3,4-c]pyrroles (DPPs) comprise a class of fluorescent dyes known for their photochemical stability, strong visible absorption, and relatively high carrier mobility.[1] These materials have been widely studied for organic electronics applications such as field effect transistors and photovoltaic devices.[1c, g, 2] With structural modifications available through either sidechain substitution at the 2,5-N-lactam position, or variation and extension of the 3,6-aryl groups, the electronic properties can be tuned through straightforward synthetic procedures.[1a, e, 3] Crystalline DPPs typically assemble through hydrogen bonding and p–p interactions into a herringbone arrangement, which maximizes intermolecular donor–acceptor interactions.[4] As a result, structural modifications strongly affect the electronic properties of DPP in the solid state.[1b, d, f,4–5]

Recently, our group determined that DPP derivatives undergo singlet exciton fission (SF) with >100 % yield,[6] a process in which two triplet excitons are produced in a[7] spin-allowed manner following absorption of a single photon. This process is possible when an assembly of two or more organic chromophores satisfying the energetic requirement $E(S_1) \geq 2\,E(T_1)$, where $E(S_1)$ is the energy of the singlet excited state and $E(T_1)$ that of the triplet excited state, have appropriate electronic coupling to form a correlated triplet pair state $^1(T_1T_1)$. Because this state has overall singlet spin configuration prior to dissociation, its formation is spin-allowed and can occur as fast as 10^{14} s$^{@1}$, which is much faster than spin-orbit-induced intersystem crossing. SF can yield two electron–hole pairs per absorbed photon as well as take advantage of the longer exciton diffusion lengths of triplet excitons. In theory, SF can overcome the 33 % Shockley–Queisser efficiency limit for single junction photovoltaics,[8] and thus, over the last decade there has been increasing interest in developing SF chromophores for enhancing photovoltaic performance.[9]

In 3,6-bis(thiophen-2-yl)diketopyrrolopyrrole (TDPP), the energetic requirement for SF is met as $E(S_1) = 2.25$ eV and $E(T_1) \leq 1.1$ eV.[6b] We have previously characterized SF in thin films of several TDPP derivatives, which takes place through an excimer-like intermediate we assigned to $^1(T_1T_1)$, but the heterogeneity of polycrystalline thin films prevents a deeper investigation into the states participating in the SF process. We also observed that replacement of the 2,5-N-alkyl sidechains with triethyleneglycol (TEG) leads to marked spectral differences, and speculated that TEG may enhance the dielectric environment of the TDPP film.[10] We therefore sought to study a covalent molecular dimer of TDPP, which enables more precise control over geometry and intermolecular coupling as determined by the bridging linker.[11] Recent work attempted to induce intramolecular SF by linking TDPP chromophores through a vinyl group, but was unsuccessful because conjugation through the

[a] C. M. Mauck, Y. J. Bae, M. Chen, N. Powers-Riggs, Dr. Y.-L. Wu, Prof. M. R. Wasielewski
Department of Chemistry
Argonne-Northwestern Solar Energy Research (ANSER) Center
Institute for Sustainability and Energy at Northwestern
Northwestern University
Evanston, IL 60208-3113 (USA)
E-mail: m-wasielewski@northwestern.edu

5-thiophene position caused the molecule to behave as one chromophore.[12]

Since SF requires a minimum of two electronically coupled chromophores to take place, molecular dimers have been commonly used to model it.[7, 11, 13] Many theoretical models are based on crystal structure dimeric geometries, and experimen-tally, recent progress has been made towards high-yield SF in covalently-linked dimers of tetracene, pentacene, and terryle-nediimide (TDI).[14] Furthermore, dimers can be studied in solu-tion, making it possible to explore the effect of the dielectric environment on the efficiency and mechanism of SF by varying the solvent polarity. In particular, charge-transfer (CT) states are thought to play an important role in the SF mechanism by serving as higher-lying virtual states that couple the initially ex-cited $^1(S_1S_0)$ state to the $^1(T_1T_1)$ state via a superexchange inter-action.[11, 15] Furthermore, the adiabatic $^1(S_1S_0)$ and $^1(T_1T_1)$ states may be more accurately understood as mixtures of the pure S_1 and T_1 states with CT configurations.[16] For example, the strong visible absorption band of DPP has been assigned to a HOMO!LUMO p!p* intramolecular CT band resulting from the interaction of the electron-rich aryl rings and electron-poor diketopyrrolopyrrole core.[17] Moreover, DPP often packs in the solid state through p–p interactions and hydrogen bonding to maximize intermolecular donor–acceptor interactions.[4] We found that greater intermolecular donor–acceptor interactions resulting from TDPP packing leads to faster $^1(T_1T_1)$ formation, indicating that CT states or configurations are important for TDPP SF. We recently reported on a TDI dimer in which the two TDI molecules are attached to a triptycene spacer in a p– p slip-stacked arrangement. In polar solvents, this dimer under-goes symmetry breaking charge separation to produce an ion pair (IP) state, while in low polarity solvents, the dimer under-goes rapid SF. Thus, if charge transfer between the two TDI molecules is stabilized by a high polarity solvent, a real IP state forms that acts as a trap for the excitation, while in low polari-ty solvents it acts as a virtual state that promotes SF.[14g] This study and others have demonstrated the value of model sys-tems for directly characterizing the states relevant to SF.

Herein, we describe the synthesis of a covalent TDPP dimer and characterize the interplay between the coupled chromo-phore excited states and the $TDPP^+C–TDPP^@C$ IP state that forms by symmetry-breaking charge separation. The two TDPP chromophores are attached at the 4-thiophene carbon to the 4,5 positions of 2,7-di-tert-butyl-9,9-dimethylxanthene (Xan), which orients the molecules in a cofacial arrangement.[18] Through-space p–p interactions between the two chromo-phores mimic interchromophore interactions in thin solid films. Using femtosecond transient absorption spectroscopy, we find that the dimer undergoes a structural rearrangement to a con-formation with enhanced CT character prior to formation of the IP state in polar solvents; however, in low polarity solvents, the IP state is destabilized and the dimer relaxes back to the excited state. Although fluorescence from the dimer is strongly quenched, we do not observe triplet formation in this TDPP dimer, highlighting the importance of both appropriate inter-molecular coupling and the entropic contribution for efficient SF in iso- or endoergic SF chromophores. Although the CT pathway prevents SF, this dimer serves as a useful molecular system for characterizing the $TDPP^+C–TDPP^@C$ state directly, and advancing our understanding of the role of CT states in DPP SF.

2. Results and Discussion

2.1. Structural Characterization

The synthesis and structure of monomer TDPP1 is shown in Scheme 1, along with dimer TDPP2. Molecular dimers have precisely defined intermolecular linkages, but in a solvated en-vironment they will experience structural fluctuations which may affect the intermolecular coupling. Variable-temperature (VT) NMR confirms the likelihood of conformational flexibility in TDPP2, even though we cannot distinguish distinct isomers. Such flexibility has been observed in xanthene-bridged chro-mophore systems previously.[18e, 19] Reporter methyl groups on the xanthene bridge have been used to determine the pres-ence of isomers in similar molecular dimers which caused peak broadening.[18e] However, broadening of the methyl reporter resonance in TDPP2 as the temperature is lowered to @40 8C is negligible (see Figures S1–S2 in the Supporting Information). As the p system of TDPP is smaller than large planar aromatic molecules like perylene, we anticipate that these reporter groups are too far from the TDPPs to experience magnetic ani-sotropy due to conformational isomers. The only strongly broadened peak is the doublet at d =9.07 ppm, which shifts to 9.21 ppm at low temperature and broadens significantly; as-signment of this proton based on 2D NOE (Figure S3) indicates that this represents the proton at the 3-thiophene carbon, on the ring attached directly to Xan through the 4-thiophene carbon. This proton participates in H-bonding with the carbon-yl oxygen and is coupled through space to the $N\text{-}CH_2$ protons on the hexyl chain of the adjacent TDPP. It follows that as this proton is the most embedded within the dimer structure, it would be most affected by conformer orientations whose in-terconversion slows as temperature decreases.

We also employed density functional theory (DFT) to calcu-late the ground-state energy of TDPP2 in a cis conformation, where the TDPP molecules face the same direction as in the crystal structure; and in a trans conformation, with the TDPPs with opposite orientations with respect to the Xan linker. The energies and structures for this calculation are provided in the Supporting Information. We employed the B3LYP functional without dispersion correction and find that the energy differ-ence between the two conformers is only 0.07 eV.

Single crystal growth and structure determination was per-formed to interpret the most thermodynamically favorable structure for the TDPP2 dimer, that is, the most stable intramo-lecular packing between TDPP units. The monoclinic structure of the TDPP2 crystal belongs in the centrosymmetric C2/c space group. The xanthene spacer is disordered at two posi-tions along the b axis on either side of the TDPP chromophore, each position exhibiting one quarter occupancy for each atom. Despite the disorder in the spacer, the TDPP ordering is strong, appearing as regularly spaced dimer units which define the in-

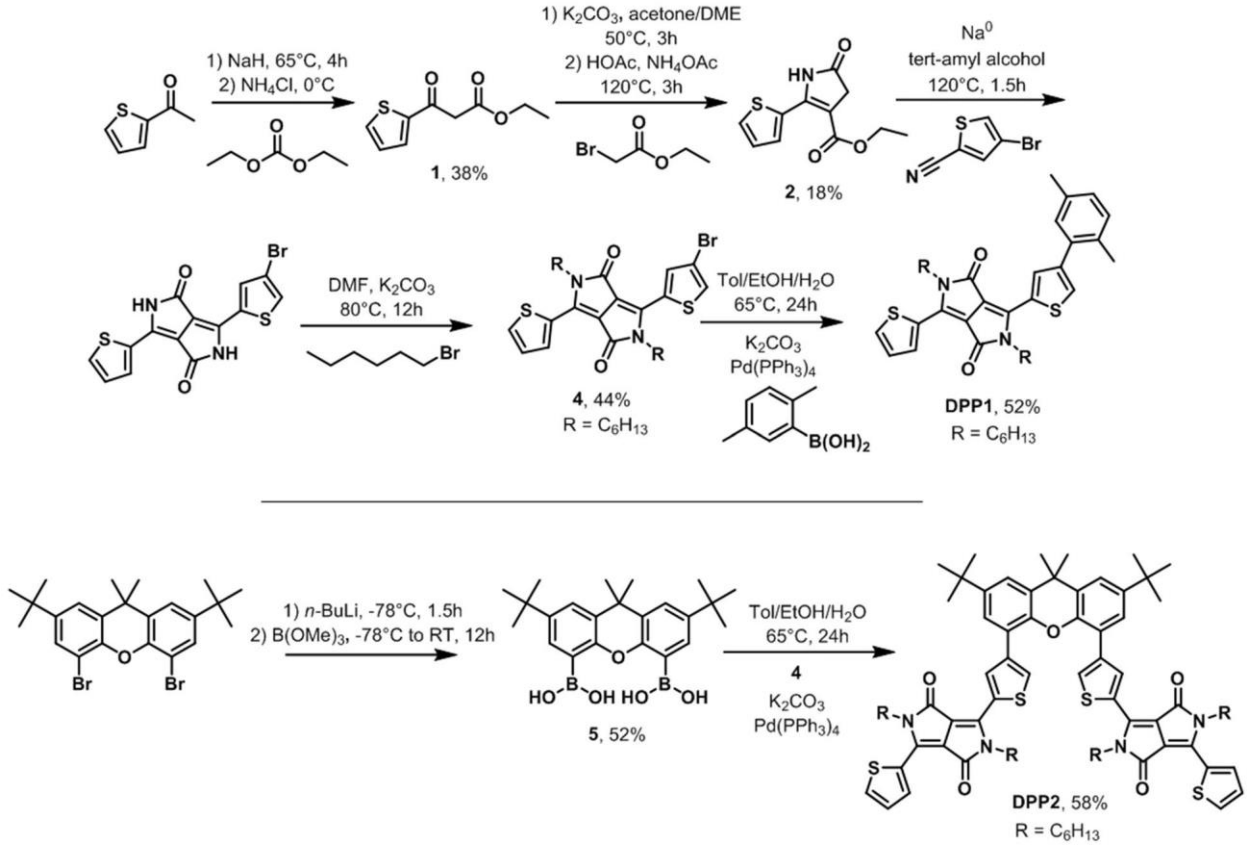

Scheme 1. Synthesis of TDPP1 and TDPP2. DME =dimethoxyethane, tol =toluene.

tramolecular p–p stacking distance, analogously to other crys-talline TDPPs.[1b, f,5c, 6b] In the TDPP2 single crystal, the p–p dis-tance is 3.37 & (Figure 1) and should lead to strong interchro-mophore coupling, as was seen in N-methyl substituted TDPP (MeTDPP) crystals with a p–p distance of 3.27 &.[6b] However, in MeTDPP, the packing leads to strong donor–acceptor interac-tions. Here, the offset along the long axis (from thiophene to thiophene 5-carbon) is 3.14 &, and 0.586 & along the short axis (connecting the carbonyl carbons). The result of this geometry is in fact somewhat slip-stacked, but the packing offsets the donor–acceptor interchromophore interaction so that adjacent rings do not strongly overlap.

2.2. Steady-State Absorption and Emission

Linkage of TDPP to Xan through the 4-thiophene carbon was chosen in order to decrease the effective conjugation between the thiophene and bridge, given that aryl substitution at the more reactive 5-thiophene position is commonly used to lower the energy of DPP derivatives by extending the conjuga-

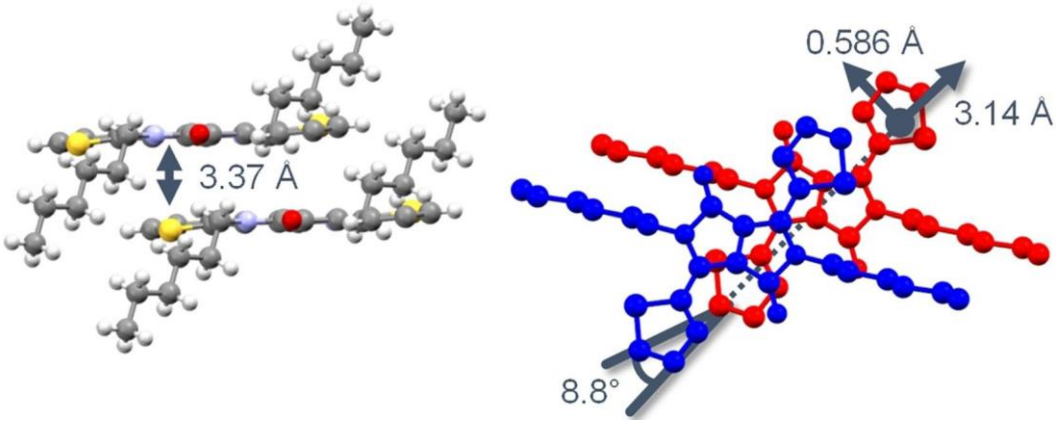

Figure 1. Interchromophore packing in the TDPP2 crystal structure, showing the p–p distance between DPP planes (left) with yaw angle and offset along the long and short axes (right). The xanthene moiety is not shown due to disorder.

tion.[1a, 20] This isomer results in minimal perturbation of the TDPP chromophore S_1 energy ($E(S_1)$ =2.25 eV) resulting in an S_1 energy for TDPP2 of 2.22 eV, as determined by the crossing point between the absorption and emission spectra in Fig-ure 2.[6b, 17] To determine whether this small shift was a result of Xan phenyl substitution or interchromophore coupling, TDPP1 was synthesized as a control. The vibronic progression in the absorption and emission spectra are essentially identical to TDPP[6b] but with $E(S_1)$ slightly red-shifted to 2.22 eV, suggest-ing that the energy difference between TDPP and TDPP2 is primarily a result of phenyl substitution and less so interchro-mophore coupling. However, the latter effect results in broad-ening of the TDPP2 absorption band, with a tail extending to l =600 nm. The intensity of the second vibronic peak grows relative to the first vibronic peak, indicating H-aggregate char-acter in which the transition dipole moments are oriented in a side-by-side parallel orientation.[21] The absorption and emis-sion spectra for TDPP1 in ether are given in Figure 2 a, along with the spectra for TDPP2 in butyronitrile (PrCN), dichlorome-thane (DCM), diethyl ether, and 1,4-dioxane. The solvent-de-pendent relative intensity of the 0–0 and 0–1 absorption bands as well as the 0–0 and 1–0 emission bands are given in Table 1.

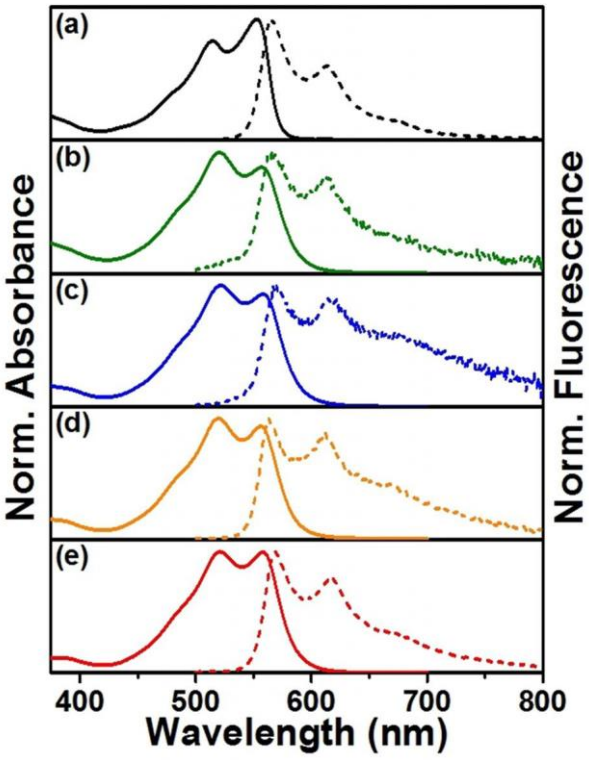

Figure 2. Normalized steady state absorption (solid line) and fluorescence (dashed line) spectra of TDPP1 in ether (a) and TDPP2 in butyronitrile (b), dichloromethane (c), diethyl ether (d), and 1,4-dioxane (e).

The fluorescence quantum yield of TDPP is high (F_F 0.74).[6a, 17] The monomer emission of TDPP1 has a similar vi-bronic character to TDPP and F_F =0.45 in diethyl ether (Figure 2). TDPP2 has strongly quenched emission, with F_F = 0.02–0.16 increasing as the solvent polarity decreases. The sol-vent dependence of the TDPP2 emission suggests that there is significant charge transfer character in its excited state, in con-trast to quenching due to H-aggregate formation. In conven-tional H-aggregates, the excited state may be stabilized in a lower-energy zero dipole configuration, the so-called excimer, which appears as a weakly emissive broad band red-shifted from the usual monomeric emission. We do not observe dis-tinct excimer emission, but note that the fluorescence ampli-tude at longer wavelengths is broadened and increased, which may originate from a minor population of excimer-like confor-mations. The increased amplitude of the TDPP2 emission at longer wavelengths is most pronounced in low polarity sol-vents where the overall emission is the weakest from CT quenching, making it more visible but never dominant as we clearly saw in thin films.[6b] The energy spacing DE between the 0–0 and 0–1 bands in the absorption spectra for TDPP2 is 1553 $cm^{@1}$, but in the emission DE is 1383, 1470, 1572, and 1592 $cm^{@1}$ for the dimer in dioxane, ether, DCM and PrCN, re-spectively. However, in TDPP2, excimer emission does not dominate the steady-state fluorescence spectra, and the overall emission resembles TDPP1 much more than the excimer-like states observed in thin films.[6] The intensity of the 0–1 band increases relative to the 0–0 band by 20 % in TDPP2 versus TDPP1 ($I(I_2):I(I_1)$ in Table 1).

2.3. Time-Resolved Fluorescence Spectroscopy

The singlet excited state lifetime of TDPP1 was measured using time-resolved fluorescence (TRF) spectroscopy following

Table 1. Steady state photophysical properties of TDPP1 and TDPP2 in different solvents.[a]

Compound	Solvent	F_F	$I_{1,abs}$ [nm]	$I_{2,abs}$ [nm]	$I(I_2):I(I_1)_{,abs}$	$I_{1,em}$ [nm]	$I_{2,em}$ [nm]	$I(I_2):I(I_1)_{,em}$
TDPP1	PrCN	0.43	551	512	0.81	562	609	0.60
	DCM	0.50	551	515	0.82	566	614	0.61
	ether	0.45	550	511	0.79	559	607	0.63
	dioxane	0.49	553	514	0.80	565	611	0.62
TDPP2	PrCN	0.024	556	520	1.15	565	613	0.79
	DCM	0.019	558	521	1.08	570	615	0.89
	ether	0.059	556	520	1.07	563	613	0.87
	dioxane	0.16	558	521	1.00	569	617	0.79

[a] Quantum yield of fluorescence (F_F), absorption peak maxima ($I_{1,abs}$ and $I_{2,abs}$), emission peak maxima ($I_{1,em}$ and $I_{2,em}$) as well as the ratio ($I(I_2):I(I_1)$) be-tween the absorption and emission peaks are given.

excitation at l =515 nm (0.2 mJ pulse$^{@1}$). The instrument response was 250 ps in an overall 20 ns time window. A fit of the monoexponential decay for TDPP1 at 575 nm yields an average lifetime of t_F =5.5 :0.5 ns, shown in black in Figure 3.

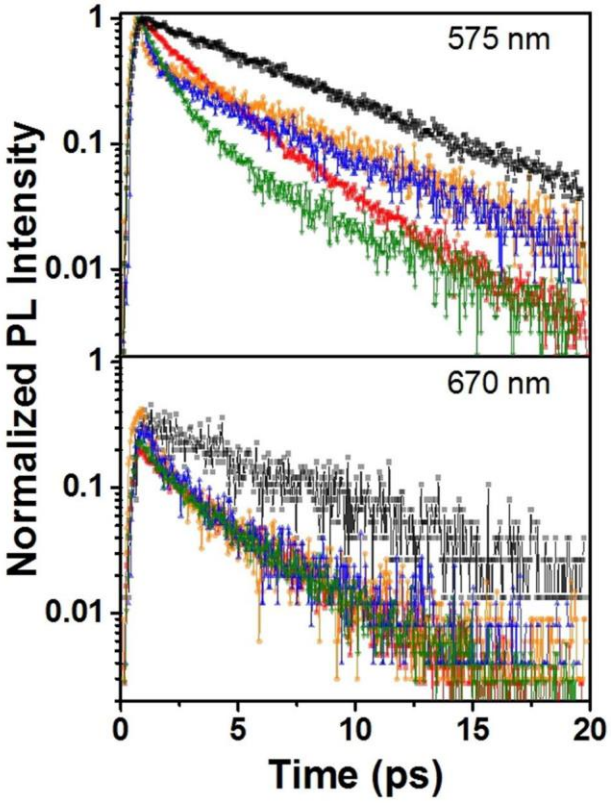

Figure 3. Fluorescence intensity decay following 515 nm excitation, at speci-fied wavelength (575 and 670 nm) for TDPP2 in 1,4-dioxane (blue), diethyl ether (green), dichloromethane (orange), and butyronitrile (red). TDPP1 given for comparison in black. Decays were normalized to the intensity at 575 nm for each solvent.

TDPP2 shows biexponential decay of the fluorescence intensi-ty at all wavelengths in all solvents studied. The kinetic decays at 575 nm (l_1) are plotted per solvent in Figure 3. The decay of the intensity at l_2 was identical to 575 nm, demonstrating no change in the relative intensity $I(l_2):I(l_1)$ from 0–20 ns. The am-plitude of the fast time component increases as solvent polari-ty decreases (0.2 ns in butyronitrile to 2.3 ns in dioxane), and the longer time component roughly corresponds to the excit-ed state lifetime of the monomer. The fast time component represents 70–90 % of the decay, as plotted in Figure 3 on a logarithmic scale. The constant and monomer-like TRF spectra of TDPP2 indicate that the fluorescence largely originates from a single state that may be in equilibrium with another non-emissive state.

The intensity at 670 nm in all solvents also displayed a biex-ponential decay, with time constants similar for all solvents, of t_1 1 ns and t_2 5 ns. This longer wavelength emission repre-sents only 20–30 % of the already weak total signal. The simi-larity across solvent polarity suggests that a weak red-shifted excimer band may be hidden under the stronger monomeric-like fluorescence. We estimate that formation of the excimer is a minor pathway for TDPP2 that can form to the same degree in all solvents due to solution-phase conformational flexibility, but has little impact on the average behavior of TDPP2. This result is somewhat surprising, given the prevalence of excimer-like emission in our previous TDPP thin film study.[22] This indi-cates that the TDPP2 geometry favors another fluorescence-quenching pathway, such as charge separation, in which the lifetime of the charge-separated IP state depends on solvent polarity.[23]

We also note that the TDPP2 emission has a vibronic signa-ture that resembles the highly fluorescent TDPP monomer, but rule out a fluorescent impurity due to the different $I(l_2):I(l_1)$ ratio between TDPP1 and TDPP2, which remains constant even at long times once the majority of the signal has de-cayed. The fits of fluorescence decay at 575, 618 nm and 670 nm are given in Figure S4.

2.4. Dimer Excited State Dynamics

Femtosecond transient absorption (fsTA) spectroscopy was performed on solutions of TDPP2 in PrCN, DCM, diethyl ether, and 1,4-dioxane to characterize the states that are formed. Ex-citation at l =560 nm (1 mJ/pulse) results in ground state bleaching (GSB) at 518 and 558 nm, and excited state absorp-tion (ESA) from 585 nm into the near-infrared (NIR) with a max-imum at 750 nm. Spectra at selected times are shown in Figure 4. In the previously studied TDPP, the S_n !S_1 transition is similar and occurs at 755 nm, but displays prominent fea-tures of stimulated emission at 606 nm.[6b] The fsTA spectra for TDPP1 are identical, and are provided for comparison in Fig-ure S5.

In TDPP2, this excited-state transition is seen at l =750–755 nm immediately after photoexcitation in all solvents. We term this state S_1S_0 which originates from the coupled chromo-phore pair and can be interpreted as the allowed vertical tran-sition from Kasha's exciton model.[21a] We do not expect to ob-serve intraband transitions between the upper and lower exci-ton states directly,[24] as the instrument response function of these experiments is 300 fs. The stimulated emission feature is reduced to a weak inverted signal on top of the ESA around 610–617 nm, the intensity of which corresponds to F_F in each solvent. The early time spectra for TDPP2 are given in Fig-ure S6.

The decay of the S_1S_0 peak is accompanied by the rise of a broad peak at 640 nm. The intensity and growth of this peak compared to the S_n !S_1S_0 transition depends strongly on sol-vent polarity. The radical cation and anion peaks for TDPP mo-nomer have been previously measured using spectroelectro-chemistry, demonstrating that TDPP$^+$C has a broad absorption centered at 605 nm with a sharp absorption band for TDPP$^{@}$C at 636 nm.[25] For TDPP2 in PrCN, the feature at 640 nm is dominant by 25 ps, when the GSB begins to decay along with the peak at 640 nm. Due to the high dielectric constant of PrCN (e =20.7) we anticipate symmetry-breaking charge sepa-ration is favorable and the TDPP$^+$C–TDPP$^{@}$C IP state is formed. Cyclic voltammetry of TDPP2 in PrCN supports this conclusion,

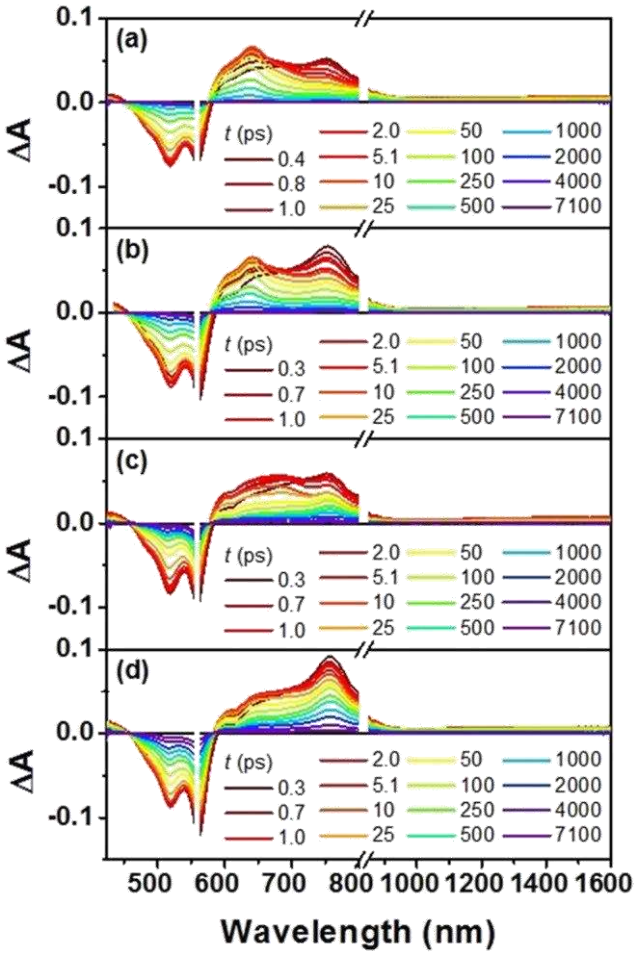

Figure 4. Femtosecond transient absorption spectra from l =450–1600 nm at selected times after photoexcitation at 560 nm for TDPP2 in butyronitrile (a), dichloromethane (b), diethyl ether (c), and 1,4-dioxane (d).

in which the difference in oxidation and reduction potentials yields 2.08 eV; the energy of the IP (E_{IP}) will be further lowered in polar solvents, due to the Coulombic contribution. The vol-tammogram is provided in Figure S7. Constrained DFT calcula-tions allow us to more accurately estimate E_{IP}, indicating that in PrCN E_{IP} is lower than the excited state by 0.17 eV (2.04 eV; B3LYP/6-31G*). Therefore the 640 nm feature peaked at 640 and the broad absorbance from 575–715 nm is assigned to the IP state.

In DCM (e =8.93), DFT calculations yield E_{IP} =2.08 eV. The decay of S_1S_0 is also accompanied by the rise of the IP band at 640 nm; however, by 10 ps the amplitude at 640 nm reaches its maximum, with a substantial amount of S_1S_0 ESA remaining. The two peaks decay simultaneously, indicating the presence of both S_1S_0 and $TDPP^{+}C–TDPP^{@}C$.

In nonpolar solvents the distinct $TDPP^{+}C–TDPP^{@}C$ band is not observed, which is in agreement with DFT calculations where E_{IP} =2.16 eV in ether and 2.58 eV in dioxane for TDPP2. In ether (e =4.33), a broad feature centered at 693 nm rises as the 750–755 nm peak decays, with weak stimulated emission overlaid. We term this state the CT state to distinguish it from the fully charge-separated IP state. This state has enhanced amplitude where the radical cation and anion of TDPP absorb, and can be thought of as partially charged, that is, $TDPP^{d\ +}–TDPP^{d}$. This band decays so that by 100 ps in ether, the spec-tra resemble S_1S_0 ESA again.

In dioxane (e =2.21), S_n !S_1S_0 transition intensity reaches a maximum at early times and decreases in intensity with the growth of a weaker shoulder centered 660 nm. The intensity of this CT absorption is the weakest of all four solvents, as ex-pected for the lowest polarity solvent studied. As was the case in ether, this shoulder decreases at late times relative to the in-tensity at 755 nm, so that the S_1S_0 ESA remains.

Probing in the NIR can reveal low-energy transitions such as those from an excimer state to a higher energy CT state, due to the charge resonance and exciton resonance contributions in the excimer.[18c, 26] This NIR Frenkel exciton-to-CT transition has been observed in perylene, and perylenediimide dimers, in the NIR to shortwave IR regions.[18c, 22, 26–27] In perylenediimide this band is predicted to be centered around 0.5 eV, because the energy of the excimer lies below the S_1 state and the energy of the charge transfer state lies above it.[28] In the case of TDPP2, we observe the rise of the IP state or the CT state around 640 nm, depending on the polarity of the solvent, im-plying that the state $^{1}(M^{+}@M^{@})$ is much closer in energy to the S_1S_0 state. In this case, the $^{1}(M^{+}@M^{@})$ configuration is directly populated, instead of acting as a virtual state. Therefore it is not surprising that the NIR spectra reveal little about the excit-ed state dynamics in TDPP2, with a broad weak absorption ex-tending across the window of detection (850–1600 nm). Even in the low dielectric environment of ether and dioxane, where the CT state is raised in energy above S_1, this transition is not observed; we speculate that the intermolecular geometry to form the excimer cannot be accessed by a majority of TDPP2 molecules in solution. Were excimer states a major population, the fluorescence would be dominated by the red-shifted, broad emission seen in our previous thin film study of TDPP.[6b] Weaker NIR bands corresponding to the TDPP IP have been measured using spectroelectrochemistry at l =831, 855, and 937 nm,[25] so some absorption in the NIR is to be expected in this molecular system that can easily take on charge transfer character. However, similar to the steady state results, we find that any spectroscopic contribution from excimer species in TDPP2 is negligible.

2.5. Global Analysis of TDPP2 Excited State Dynamics

A global kinetic analysis was performed on the two-dimension-al visible-region fsTA datasets for TDPP2 to interpret the dimer photophysics in different solvents using a custom MATLAB pro-gram. In this analysis, a proposed kinetic model is fit to select-ed wavelengths and the fit parameters are varied in order to solve the set of differential equations associated with the model. For TDPP2, the identity of the species depends on the dielectric constant of the solvent, but in each case the simplest model consisted of three proposed states, A, B, and C, which are populated in a stepwise manner A!B!C followed by decay to the ground state (GS). We have not explicitly included alternative decay pathways in this analysis, such as excimer for-

mation, which we deem a minor pathway, and the resulting fit represents effective rate constants that incorporate contributions from radiative decay and other pathways for population loss. Therefore the differential equations for modeling the data are [Eqs. (1)–(3)]:

d½A& k A 1
dt ¼@ 1½ ð Þ

d½B& k A k B 2
dt ¼ 1 &@ 2 ð Þ

d½C& k B k C 3
dt ¼ 2½ &@ 3½ & ð Þ

The resulting normalized species-associated spectra for each solvent are given in Figure 5, and the associated globally fit multiple wavelength kinetic traces and non-normalized spectra are presented in Figure S9. In all cases, the ESA of the initial species A extends from 580 nm to the edge of the visible detection window and maximizes between 750–755 nm. Specie-s A represents the S_1S_0 state prior to reorganization of either the solvent shell or the molecular structure, which presumably increases the asymmetry of the dimer structure and results in the development of CT character ($TDPP^{d+}$–$TDPP^{d@}$), which is a function of solvent polarity. Hence the degree of IP formation can be seen in species B, where the intensity of the peak at 640 nm has the expected dependence on solvent polarity. The ratio of this peak to the relative intensity of the S_1S_0 ESA for species B in each solvent (A_{640} :A_{750}) ranges from 2.3 for PrCN, 1.4 for DCM, 1.2 for ether, to 0.65 for dioxane.

The identity of species C varies with solvent polarity. The accessibility of the IP state is dictated by how much its energy is stabilized by the polar solvent environment, and thus in PrCN this state falls below E(S_1) and species C is the fully charge separated IP state. The spectra for species C comprises ESA for the IP state in PrCN and DCM after some relaxation step from the CT state, and the kinetic model to fit the datasets in polar solvents is S_1S_0 !CT!IP. In PrCN the IP spectrum is the primary component of species C, whereas in DCM, the spectrum of C sharpens through loss of amplitude between 660–690 nm as the IP state is formed, with a weak peak at 750 nm remaining. In ether and dioxane, the final species recovers the stimulated emission at 615 nm, and loses most of the broad shoulder of the CT state. In low polarity solvents the energy of the IP state is above the S_1S_0 state, so that the CT state cannot evolve along the potential energy surface towards the fully charge separated IP state and instead relaxes back towards a state re-sembling S_1S_0. In this instance, the kinetic model to fit the da-tasets is S_1S_0 !CT!(S_1S_0)'. The small spectral differences be-tween the initial and final states indicate that (S_1S_0)' has a slightly different geometry than the initially excited state gen-erated from the vertical transition, perhaps stabilized by in-creased coupling from the chromophores being closer togeth-er.[22, 28a] In the present work we focus on the time-resolved electronic spectra of TDPP2 but further study of the dimer with time-resolved vibrational spectroscopy could help eluci-date the structural dynamics associated with the (S_1S_0)' state.

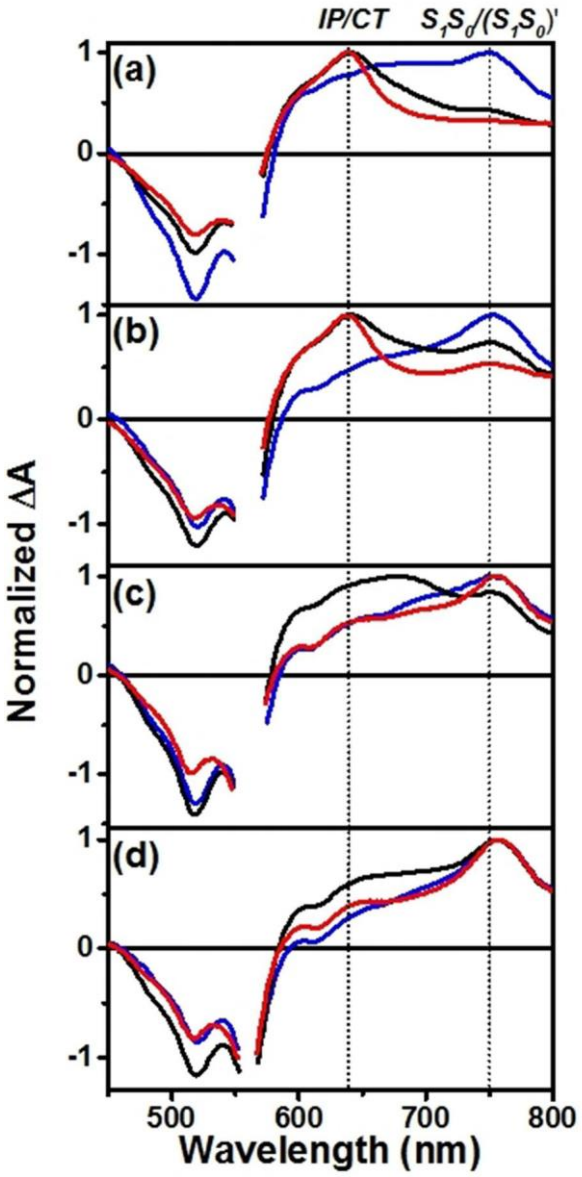

Figure 5. Species-associated spectra from global analysis to a three-state S_1S_0 !CT !IP or (S_1S_0)' kinetic model for TDPP2 in butyronitrile (a), dichloromethane (b), diethyl ether (c), and 1,4-dioxane (d). S_1S_0 =blue, CT =black, IP/(S_1S_0)' =red. Dotted lines provided at 640 and 750 nm as a guide to the eye.

The globally fit time constants for decay of Species A (S_1S_0), B (CT), and C (IP or (S_1S_0)') are summarized in Table 2 for each solvent. The effective time constant for CT state formation is on the order of several picoseconds, which is reasonable for solvent reorganization or a geometric relaxation. In all solvents decay of the CT state takes place in t 70 ps either to the IP state or to (S_1S_0)'. The effective decay time constant for the final species depends on charge recombination (CR) of $TDPP^{+}C$–$TDPP^{<M-}C^{>}$ or $TDPP^{d+}$–$TDPP^{d@}$ combined with radiative decay from (S_1S_0)'.

2.6. Pseudoequilibrium between the S_1S_0 and CT States

Based on the fsTA spectra as well as the biexponential, monomer-like TRF decays, we propose that an equilibrium exists be-

Table 2. Globally fit time constants in picoseconds for TDPP2 in different solvents following the proposed kinetic model S_1S_0 !CT!IP in DCM and PrCN, or S_1S_0 !CT!(S_1S_0)' in ether and dioxane.[a]

Solvent	t_1 [ps]	t_2 [ps]	t_3 [ns]	$K_{eq'}$	t_1' [ps]	$t_{@1}$ [ps]
PrCN	2.3 :0.3	48.2 :0.7	0.70 :0.01	2.77	3.1	9.4
DCM	1.7 :0.3	72 :1	1.04 :0.01	1.45	0.5	1.1
ether	0.8 :0.3	12.0 :0.3	2.13 :0.03	0.54	2.3	1.2
dioxane	1.1 :0.3	19.7 :0.3	2.61 :0.03	0.42	3.4	1.4

[a] t_1 =decay of S_1S_0, t_2 =decay of CT, and t_3 =decay of IP or (S_1S_0)' to the ground state. Estimated equilibrium time constants are also provided (t_1' and t_{-1}') along with the estimated equilibrium constant for each sol-vent K_{eq}" [CT]/[S_1S_0] at t_{eq}.

tween the CT state and the initially photoexcited state S_1S_0 that is mediated by a geometric rearrangement of the dimer that increases its CT character. Such equilibria have been seen before in dimers undergoing symmetry breaking charge sepa-ration.[19, 29] However, this equilibrium does not persist in TDPP2, and instead falls back to whichever state is more stable depending on the solvent environment, that is, IP or (S_1S_0)'; a more proper term for this, then, is a pseudo-equilibrium.

Nuclear motion leading to more stable intermolecular interactions has been observed previously in cofacial dimers of perylenediimide derivatives bridged by similar linkers.[18c, d, 22, 27, 28b] Conformational isomers have also been observed in perylene dimers.[18e] In these cases excimer formation occurs, showing a broad, featureless and red-shifted emission band with a life-time that is typically an order of magnitude longer than the monomer. The formation of this species can be observed using picosecond TRF, as the monomer fluorescence decays and the excimer formation grows in. In the case of TDPP2; however, the TRF spectra do not change from 0–20 ns. Instead, the spec-tra maintain approximately the same vibronic band ratio seen in the steady state fluorescence spectra, which do not have a clear excimer emission band. Given the spectra and the long-component decays that correspond to the monomer excited state lifetimes in all solvents, we consider a pseudoequilibrium S_1S_0QCT!(S_1S_0)' that is modulated by fluctuations in the molecular geometry. The equilibrium constant therefore depends on solvent polarity.

We have attempted to estimate an equilibrium constant for each solvent by assuming that the concentration of [S_1S_0] and [CT] should be proportional to the absorbances A_{750} and A_{640}, respectively, although we acknowledge that this assumption does not consider differences in extinction coefficients be-tween the species. However, as this ratio should be proportion-al to K_{eq} the decay at each wavelength was used to plot A_{640}/ A_{750} (i.e. [CT]/[S_1S_0]) and determine at what time (t_{eq}) this curve is flat. The relative intensities at t_{eq} for A_{640}/A_{750} are then used to calculate an estimated K_{eq}", resulting in 2.77, 1.45, 0.54, and 0.42 for PrCN, DCM, ether, and dioxane, respectively. Using the estimated value for K_{eq}", the fsTA data were fit to a kinetic model S_1S_0QCT where k_1 is the forward rate and the backward rate $k_{@1}$ =(1/ $K_{eq'}$) 0 k_1. From this fit, the estimated time constants t_1' and $t_{@1}$' are derived, which are summarized in Table 2.

We note that the resulting rate matrix still remains underdetermined, as the two eigenvalues representing the effective rate constants for the equilibrium step depend on three rates k_1, k_{-1}, and k_2. The differential equations, species-associated spectra, kinetics, and further details are given in the Support-ing Information for the estimated pseudoequilibrium fit. The results of this model underscore the dependence of the pseudoequilibrium on stabilization of the CT state.

2.7. Origin of Symmetry Breaking in TDPP2

Optimized geometries from DFT calculations for the ground state and the charge-separated state computed in DCM are compared in Figure 6, with an energy diagram for proposed

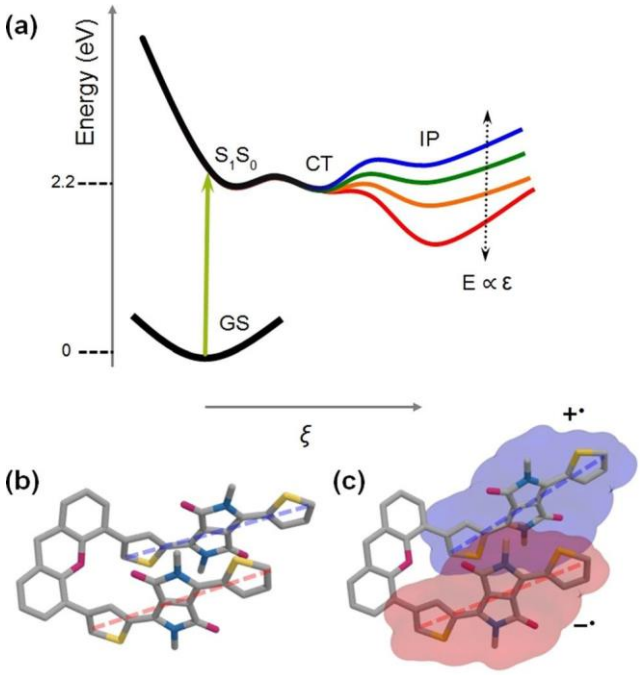

Figure 6. a) Schematic diagram for the kinetic model used to fit TDPP2 fsTA data. S_1S_0 =initially excited state, CT =$TDPP^{d+}$–$TDPP^{d@}$, IP =$TDPP^{+}C$–$TDPP^{@}C$. b) Optimized ground state geometry and c) ion-pair state for TDPP2, e =8.93. Dotted lines are provided along the TDPP thiophene–thiophene axis as a guide to the eye.

motion along a reaction coordinate that imparts greater charge transfer character to the dimer in Figure 6 a. In the ground state, both TDPPs in the dimer are planar to one another. However, in Figure 6 b, the IP state loses this planarity as the angle between the chromophores increases, with a corre-sponding change in the xanthene–thiophene torsional angle. These computed structures are plausible for the conformation-ally flexible TDPP2 in which torsional motion would impart the needed asymmetry for charge separation.

2.8. Absence of Singlet Fission in TDPP2

In our previous study, we observed fast triplet formation in TDPP thin films with a 70–200 % yield, in contrast to the <1 % intrinsic intersystem crossing of the monomer in solution.[6b] Here, TDPP2 does not form a detectable amount of triplet within the timescale of the fsTA experiment, with an absence of a positive feature around 580–600 nm and negative features at 550–580 nm and 600–620 nm.[6b] We envision several likely reasons for the difference between the thin films and this xan-thene-bridged dimer. The first is that the degree of CT charac-ter of the dimer is much greater than in the thin film, even in dioxane, perhaps due to conformational degrees of freedom available in solution that are frozen out in thin films. Instead of forming the correlated triplet pair $^1(T_1T_1)$, the dimer can rear-range to the partially charge separated state $TDPP^{d+}$–$TDPP^{d@}$, which then either leads to IP formation or back to (S_1S_0)'.

When dissolved in a highly viscous solvent of low polarity such as paraffin oil, we can study the dimer in solution but with slowed molecular fluctuations. In this case, the initially photoexcited state most resembles the CT states observed in the species-associated spectra for TDPP2 in dioxane and ether (Figure S8), then cleanly evolves to (S_1S_0)' with a pronounced stimulated emission feature analogous to the monomeric local-ly excited state (Figure S5). These results in viscous solution suggest that thermal fluctuations govern the degree of inter-molecular interaction, which modify the extent of CT character and subsequent (S_1S_0)' emission, in agreement with our pseu-doequilibrium model.

In our previous study of TDPP thin films we observed that packing arrangements that enhanced intermolecular donor–ac-ceptor interactions between thiophene rings and diketopyrro-lopyrrole cores lead to higher triplet yields.[6b] In another DPP film study with phenylthiophene, phenyl, and thiophene-sub-stituted derivatives, SF was also highly efficient.[6a] We have in fact observed triplet formation in every DPP derivative thin film that we have studied. It is therefore surprising that in TDPP2 no triplet is observed. This may be due to the impor-tance of interchromophore geometry.[14a, b, g, 15b,30] The so-called Goldilocks electronic coupling, modulated by that geometry, must not be too strong or too weak.[7,27a, 31] Although charge separation is favorable due to symmetry breaking, the orbital overlap between adjacent TDPPs may not be favorable for SF, as it lacks the strong thiophene-core interaction that is thought to promote SF in TDPP thin films. Recently, a symme-try-breaking phonon mode was proposed to activate vibronic coupling in rubrene crystals and drive coherent singlet fis-sion.[32] The authors of this study noted the importance of a $^1(S_1S_0)$–$^1(T_1T_1)$ conical intersection in the Franck–Condon region for this coherent SF to occur, underscoring previous findings in TIPS-pentacene.[33] However, symmetry breaking charge trans-fer is common in organic chromophore pairs depending on solvent polarity, as has been well-documented.[34] Depending on the molecular system, symmetry breaking charge separa-tion may also compete with SF depending on the position and relative energies of the S_1S_0, $^1(T_1T_1)$, and IP states. In the case of TDPP2, the CT state forms following reorganization after pho-toexcitation, and closes out the possibility of SF triplet formation.

Finally, in the case of TDPP2, the entropic contribution to SF must be considered.[35] SF is enthalpically favorable when DE_{ST} $2E(T_1)$–$E(S_1)$ 0, which is satisfied for TDPP (2 0 1.1 eV–2.25 eV). In pentacene SF is significantly exoergic and intramo-lecular SF has been achieved in several pentacene dimers.[14a, c, e] On the other hand, for tetracene derivatives, the enthalpic con-tribution to DG_{SF} is slightly endo- or isothermic, and the entro-py gain by separating two triplets has been proven crucial to high yield SF. In a recent paper, separated triplets could not be formed in an isolated tetracene dimer, but in a tetracene matrix the dimer could separate the $^1(T_1T_1)$ state through trip-let energy transfer.[14b] Indeed, the thin film environment and the dimer differ greatly in terms of entropy, because in the thin film a large number of states N are accessible from triplet formation defined by the Dexter radius,[35b] whereas the dimer geometry confines N to only two chromophores. We note that high yield SF in molecular dimers has, to our knowledge, only been observed thus far for the exoergic SF chromophores pen-tacene and TDI.[14a, e, g] In thin films, TDPP readily undergoes SF in 70–200 % yield;[6] due to the absence of any triplet forma-tion here despite strong p–p interchromophore interaction that mimics thin films, we conclude that the entropic contribu-tion is key when DE_{ST} is close to zero, as has been invoked in tetracene.[14b,35b] With no strong driving force for SF, a CT state close in energy to S_1, and a geometry that does not enhance appropriate orbital overlap, it is perhaps not surprising then that TDPP2 does not undergo SF.

3. Conclusions

Characterizing CT states in SF chromophores is important for understanding and interpreting spectroscopic studies on the SF mechanism. We have therefore synthesized a molecular dimer of TDPP bridged by Xan to mimic thin film p–p interac-tions, TDPP2. Using femtosecond transient absorption spec-troscopy and time resolved fluorescence spectroscopy, we have characterized the excited state dynamics of TDPP2, which undergoes symmetry-breaking charge separation in polar solvents through a partially charged CT state. The IP state is not stabilized by nonpolar solvents, and although molecular reorganization leads to an intermediate CT state, it is unable to form the fully charge separated IP. Instead, the excited state re-laxes back to the (S_1S_0)' state. In all solvents, we observe a pseudoequilibrium between S_1S_0 and the CT state, which leads to monomer-like fluorescence. Although TDPP has favorable energetics for SF in the thin film and TDPP2 clearly has strong CT character, we do not observe the formation of either the $^1(T_1T_1)$ or free triplet states in this dimer. This solution-phase dimer study highlights the importance of intramolecular cou-pling as well as the importance of entropy to promoting SF in chromophore dimers for which SF is endo- or isoergic.

Experimental Section

Synthesis

All chemicals and solvents were purchased from Aldrich, apart from 4-bromothiophene carbonitrile, which was obtained from Matrix Scientific. The synthesis of 4 and TDPP1 followed published procedures for asymmetric DPPs via thiophene pyrrolinone ester.[36] Xanthene bis-boronic acid 5 was synthesized according to the literature,[18f] and coupled with 4 to provide TDPP2. Products were purified by column chromatography and stored in the dark. The variable temperature ^{1}H NMR spectra were recorded on a Bruker Avance III 600 MHz spectrometer and the 2D NOESY experiments were performed on an Agilent DD2 600 MHz spectrometer with an NOE mixing time of 300 ms. All other NMR spectra were acquired on a Bruker Avance III 500 MHz spectrometer. MALDI-TOF was performed on a Bruker Autoflex III in reflection mode. High-resolution ESI mass spectrometry was recorded on a Bruker Impact-II. Further synthetic details are given in the Supporting Information.

Optical Spectroscopy

Steady-state absorption spectra were acquired on a Shimadzu UV-1800 spectrophotometer. Steady-state fluorescence spectra were measured using a HORIBA Nanolog fluorimeter. Quantum yields were determined using Rhodamine 101 in acidic ethanol as a standard. Femtosecond transient absorption spectroscopy was performed using a regeneratively amplified Ti:sapphire laser at 1 kHz to generate 414 nm light through frequency doubling of the fundamental, to pump a homebuilt OPA and generate a pump pulse at 560 nm, with a portion of the fundamental focused onto sap-phire to generate continuum from 430–850 nm for the probe. To generate a NIR white-light probe from 850–1620 nm, the funda-mental could also be directed onto a proprietary medium (Ultrafast Systems, LLC). The experimental set-up has been previously de-scribed, with an instrument response function of 300 fs.[37] For pi-cosecond time-resolved fluorescence spectroscopy, a 100 kHz am-plifier Spirit 1040-4 (Spectra Physics) with 1040 nm fundamental output was used to drive a noncollinear OPA (Spirit NOPA-3 H, Spectra Physics) at 515 nm to yield a 75 fs, 0.2 mJ pump pulse. Data were collected with a streak camera (Hamamatsu C4334) having an instrument response function of 200–250 ps in a 20 ns window.

Crystal Structure Determination

Single crystals of TDPP2 were grown by slow vapor diffusion of methanol into a chloroform solution. A suitable crystal was select-ed and mounted on a microloop with paratone oil on a Bruker APEX-II CCD diffractometer. The crystal was kept at 100 K via liquid N_2 stream during data collection. Using Olex2,[38] the structure was solved with the XS structure solution program[39] using Direct Methods and refined with the ShelXL refinement package using Least Squares minimization.[40] Further information about crystallographic methods is provided in the Supporting Information. CCDC 1566773 contains the supplementary crystallographic data for this paper. These data can be obtained free of charge from The Cambridge Crystallographic Data Centre.

Computational Details

A simplified structure of DPP2 was used to reduce computational cost, by removing the tert-butyl and methyl groups of Xan and replacing the N-hexyl chains of DPP with methyl groups. Density functional theory (DFT) calculations were performed in QChem (v. 4.0) with the B3LYP functional and 6-31G* basis set. Optimized geometries were first computed in the gas phase, followed by further optimization using a polarizable continuum model (C-PCM) and the specified optical and static dielectric constants for each solvent medium. To compute the energy of the ion pair state in DPP2, constrained DFT geometry optimizations incorporating solvation were performed in which one DPP was defined as having a +1 charge with its partner having a@1 charge.[41] Convergence was reached for dielectrics of DCM, ether, and PrCN. A single point calculation on the optimized geometry in ether was then performed to obtain E_{CT} for DPP2 in dioxane. Structures and energies are provided in the Supporting Information.

Acknowledgements

This work was supported by the Chemical Sciences, Geosciences, and Biosciences Division, Office of Basic Energy Sciences, DOE, under grant no. DE-FG02-99ER14999 (M.R.W.). C.M.M. acknowl-edges the support of a NSF Graduate Research Fellowship under grant no. DGE-1324585. This work made use of the IMSERC at Northwestern University, which has received support from the Soft and Hybrid Nanotechnology Experimental (SHyNE) Resource (NSF NNCI-1542205), the State of Illinois and International Insti-tute for Nanotechnology (IIN), as well as the Northwestern Uni-versity Department of Chemistry and the Office of Research. The authors thank Charlotte Stern for assistance in single-crystal X-ray diffraction, Dr. S. Habibi Goudarzi for assistance with high-resolution mass spectrometry, and Brian Phelan for useful discussions.

Conflict of Interest

The authors declare no conflict of interest.

Keywords: electron transfer · photophysics · radical ions · singlet fission · time-resolved spectroscopy

[1] a) H. B4rckst4mmer, A. Weissenstein, D. Bialas, F. W4rthner, J. Org. Chem. 2011, 76, 2426 – 2432; b) J. Calvo-Castro, M. Warzecha, A. R. Ken-nedy, C. J. McHugh, A. J. McLean, Cryst. Growth Des. 2014, 14, 4849 – 4858; c) D. Chandran, K.-S. Lee, Macromol. Res. 2013, 21, 272 – 283; d) J. Dhar, D. P. Karothu, S. Patil, Chem. Commun. 2015, 51, 97 – 100; e) M. Grzybowski, D. T. Gryko, Adv. Opt. Mater. 2015, 3, 280 – 320; f) H. Langh-als, T. Potrawa, H. Nçth, G. Linti, Angew. Chem. Int. Ed. Engl. 1989, 28, 478 – 480; Angew. Chem. 1989, 101, 497 – 499; g) M. A. Naik, S. Patil, J. Polym. Sci. Part A 2013, 51, 4241 – 4260.

[2] a) S. Loser, C. J. Bruns, H. Miyauchi, R. P. Ortiz, A. Facchetti, S. I. Stupp, T.J. Marks, J. Am. Chem. Soc. 2011, 133, 8142 – 8145; b) S. Qu, H. Tian, Chem. Commun. 2012, 48, 3039 – 3051.

[3] a) J. Dhar, N. Venkatramaiah, A. A, S. Patil, J. Mater. Chem. C 2014, 2, 3457 – 3466; b) A. Iqbal, M. Jost, R. Kirchmayr, J. Pfenninger, A. Rochat, O. Wallquist, Bull. Soc. Chim. Belges 1988, 97, 615 – 644.

[4] J. Mizuguchi, S. Homma, J. Appl. Phys. 1989, 66, 3104 – 3110.

[5] a) M. Adachi, S. Nakamura, J. Phys. Chem. 1994, 98, 1796 – 1801; b) P. E. Hartnett, S. M. Dyar, E. A. Margulies, L. E. Shoer, A. W. Cook, S. W. Eaton, T.J. Marks, M. R. Wasielewski, Chem. Sci. 2015, 6, 402 – 411; c) M. Kirkus, L. Wang, S. Mothy, D. Beljonne, J. Cornil, R. A. J. Janssen, S. C. J. Meskers, J. Phys. Chem. A 2012, 116, 7927 – 7936.

a) P. E. Hrtnett, E. A. Margulies, C. M. Mauck, S. A. Miller, Y. Wu, Y.-L. Wu, T. J. Marks, M. R. Wasielewski, J. Phys. Chem. B 2016, 120, 1357 – 1366; b) C. M. Mauck, P. E. Hartnett, E. A. Margulies, L. Ma, C. E. Miller, G. C. Schatz, T. J. Marks, M. R. Wasielewski, J. Am. Chem. Soc. 2016, 138, 11749 – 11761.
[7] M. B. Smith, J. Michl, Chem. Rev. 2010, 110, 6891 – 6936.
[8] W. Shockley, H. J. Queisser, J. Appl. Phys. 1961, 32, 510 – 519.
[9] a) M. B. Smith, J. Michl, Annu. Rev. Phys. Chem. 2013, 64, 361 – 386; b) M. C. Hanna, A. J. Nozik, J. Appl. Phys. 2006, 100, 074510.
[10] a) J. E. Donaghey, A. Armin, P. L. Burn, P. Meredith, Chem. Commun. 2015, 51, 14115 – 14118; b) X. Liu, K. S. Jeong, B. P. Williams, K. Vakhshouri, C. Guo, K. Han, E. D. Gomez, Q. Wang, J. B. Asbury, J. Phys. Chem. B 2013, 117, 15866 – 15874.
[11] E. C. Greyson, J. Vura-Weis, J. Michl, M. A. Ratner, J. Phys. Chem. B 2010, 114, 14168 – 14177.
[12] T. Mukhopadhyay, A. J. Musser, B. Puttaraju, J. Dhar, R. H. Friend, S. Patil, J. Phys. Chem. Lett. 2017, 8, 984 – 991.
[13] F. Mirjani, N. Renaud, N. Gorczak, F. C. Grozema, J. Phys. Chem. C 2014, 118, 14192 – 14199.
[14] a) J. Zirzlmeier, D. Lehnherr, P. B. Coto, E. T. Chernick, R. Casillas, B. S. Basel, M. Thoss, R. R. Tykwinski, D. M. Guldi, Proc. Natl. Acad. Sci. USA 2015, 112, 5325 – 5330; b) N. V. Korovina, S. Das, Z. Nett, X. Feng, J. Joy, R. Haiges, A. I. Krylov, S. E. Bradforth, M. E. Thompson, J. Am. Chem. Soc. 2015, 138, 617 – 627; c) B. S. Basel, J. Zirzlmeier, C. Hetzer, B. T. Phelan, M. D. Krzyaniak, S. R. Reddy, P. B. Coto, N. E. Horwitz, R. M. Young, F. J. White, F. Hampel, T. Clark, M. Thoss, R. R. Tykwinski, M. R. Wasielewski, D. M. Guldi, Nat. Commun. 2017, 8, 15171; d) S. N. Sanders, E. Kumarasamy, A. B. Pun, K. Appavoo, M. L. Steigerwald, L. M. Campos, M. Y. Sfeir, J. Am. Chem. Soc. 2016, 138, 7289 – 7297; e) S. N. Sanders, E. Kumarasamy, A. B. Pun, M. T. Trinh, B. Choi, J. Xia, E. J. Taffet, J. Z. Low, J. R. Miller, X. Roy, X. Y. Zhu, M. L. Steigerwald, M. Y. Sfeir, L. M. Campos, J. Am. Chem. Soc. 2015, 137, 8965 – 8972; f) S. Lukman, A. J. Musser, K. Chen, S. Athanasopoulos, C. K. Yong, Z. Zeng, Q. Ye, C. Chi, J. M. Hodgkiss, J. Wu, R. H. Friend, N. C. Greenham, Adv. Funct. Mater. 2015, 25, 5452 – 5461; g) E. A. Margulies, C. E. Miller, Y. Wu, L. Ma, G. C. Schatz, R. M. Young, M. R. Wasielewski, Nat. Chem. 2016, 8, 1120 – 1125.
[15] a) C. E. Miller, M. R. Wasielewski, G. C. Schatz, J. Phys. Chem. C 2017, 121, 10345 – 10350; b) S. R. Yost, J. Lee, M. W. B. Wilson, T. Wu, D. P. McMahon, R. R. Parkhurst, N. J. Thompson, D. N. Congreve, A. Rao, K. Johnson, M. Y. Sfeir, M. G. Bawendi, T. M. Swager, R. H. Friend, M. A. Baldo, T. Van Voorhis, Nat. Chem. 2014, 6, 492 – 497; c) T. C. Berkelbach, M. S. Hybertsen, D. R. Reichman, J. Chem. Phys. 2013, 138, 114102.
[16] R. Tempelaar, D. R. Reichman, J. Chem. Phys. 2017, 146, 174703.
[17] M. A. Naik, N. Venkatramaiah, C. Kanimozhi, S. Patil, J. Phys. Chem. C 2012, 116, 26128 – 26137.
[18] a) J. M. Giaimo, J. V. Lockard, L. E. Sinks, A. M. Scott, T. M. Wilson, M. R. Wasielewski, J. Phys. Chem. A 2008, 112, 2322 – 2330; b) K. M. Lefler, K. E. Brown, W. A. Salamant, S. M. Dyar, K. E. Knowles, M. R. Wasielewski, J. Phys. Chem. A 2013, 117, 10333 – 10345; c) K. E. Brown, W. A. Salamant, L. E. Shoer, R. M. Young, M. R. Wasielewski, J. Phys. Chem. Lett. 2014, 5, 2588 – 2593; d) R. J. Lindquist, K. M. Lefler, K. E. Brown, S. M. Dyar, E. A. Margulies, R. M. Young, M. R. Wasielewski, J. Am. Chem. Soc. 2014, 136, 14912 – 14923; e) R. E. Cook, B. T. Phelan, L. E. Shoer, M. B. Majewski, M. R. Wasielewski, Inorg. Chem. 2016, 55, 12281 – 12289; f) W.-L. Tong, S.-M. Yiu, M. C. W. Chan, Inorg. Chem. 2013, 52, 7114 – 7124; g) R. Takita, C. Song, T. M. Swager, Org. Lett. 2008, 10, 5003 – 5005.
[19] D. Veldman, S. M. A. Chopin, S. C. J. Mesrs, M. M. Groeneveld, R. M. Williams, R. A. J. Janssen, J. Phys. Chem. A 2008, 112, 5846 – 5857.
[20] S. Stas, S. Sergeyev, Y. Geerts, Tetrahedron 2010, 66, 1837 – 1845.
[21] a) M. Kasha, H. R. Rawls, M. A. El-Bayoumi, Pure Appl. Chem. 1965, 11, 371 – 392; b) E. G. McRae, M. Kasha, Phys. Processes Radiat. Biol. Proc. Int. Symp. 1964, 23 – 42; c) N. J. Hestand, F. C. Spano, J. Chem. Phys. 2015, 143, 244707.
[22] C. M. Mauck, R. M. Young, M. R. Wasielewski, J. Phys. Chem. A 2017, 121, 784 – 792.
[23] a) T. J. Kang, W. Jarzeba, P. F. Barbara, T. Fonseca, Chem. Phys. 1990, 149, 81 – 95 ; b) J. M. Giaimo, A. V. Gusev, M. R. Wasielewski, J. Am. Chem. Soc. 2002, 124, 8530 – 8531.
[24] J. Sung, P. Kim, B. Fimmel, F. W4rthner, D. Kim, Nat. Commun. 2015, 6, 8646.
[25] A. Ruff, E. Heyer, T. Roland, S. Haacke, R. Ziessel, S. Ludwigs, Electrochim. Acta 2015, 173, 847 – 859.
[26] R. Katoh, E. Katoh, N. Nakashima, M. Yuuki, M. Kotani, J. Phys. Chem. A 1997, 101, 7725 – 7728.
[27] a) E. A. Margulies, L. E. Shoer, S. W. Eaton, M. R. Wasielewski, Phys. Chem. Chem. Phys. 2014, 16, 23735 – 23742; b) M. Son, K. H. Park, C. Shao, F. W4rthner, D. Kim, J. Phys. Chem. Lett. 2014, 5, 3601 – 3607.
[28] a) A. Schubert, V. Settels, W. Liu, F. W4rthner, C. Meier, R. F. Fink, S. Schindlbeck, S. Lochbrunner, B. Engels, V. Engel, J. Phys. Chem. Lett. 2013, 4, 792 – 796; b) A. Schubert, M. Falge, M. Kess, V. Settels, S. Lochbrunner, W. T. Strunz, F. W4rthner, B. Engels, V. Engel, J. Phys. Chem. A 2014, 118, 1403 – 1412.
[29] T. J. Kang, M. A. Kahlow, D. Giser, S. Swallen, V. Nagarajan, W. Jarzeba, P. F. Barbara, J. Phys. Chem. 1988, 92, 6800 – 6807.
[30] J. C. Johnson, A. J. Nozik, J. Michl, Acc. Chem. Res. 2013, 46, 1290 – 1299.
[31] J. J. Burdett, C. J. Bardeen, Acc. Chem. Res. 2013, 46, 1312 – 1320.
[32] K. Miyata, Y. Kurashige, K. Watanabe, T. Sugimoto, S. Takahashi, S. Tanaka, J. Takeya, T. Yanai, Y. Matsumoto, Nat. Chem. 2017, 9, 983 – 989.
[33] A. J. Musser, M. Liebel, C. Schnedermann, T. Wende, T. B. Kehoe, A. Rao, P. Kukura, Nat. Phys. 2015, 11, 352 – 357.
[34] E. Vauthey, ChemPhysChem 2012, 13, 2001 – 2011.
[35] a) W.-L. Chan, M. Ligges, X. Y. Zhu, Nat. Chem. 2012, 4, 840 – 845; b) A. B. Kolomeisky, X. Feng, A. I. Krylov, J. Phys. Chem. C 2014, 118, 5188 – 5195.
[36] a) T. Aysha, S. Lun˘Qk Jr, A. Lyc˘ka, J. Vyn˘uchal, Z. EliQs˘, A. Ru˚z˘ic˘ka, Z. Pade˘lkovQ, R. Hrdina, Dyes Pigm. 2013, 98, 530 – 539; b) S. Stas, J.-Y. Balandier, V. Lemaur, O. Fenwick, G. Tregnago, F. Quist, F. Cacialli, J. Cornil, Y. H. Geerts, Dyes Pigm. 2013, 97, 198 – 208.
[37] R. M. Young, S. C. Jensen, K. Edme, Y. Wu, M. D. Krzyaniak, N. A. Vermeulen, E. J. Dale, J. F. Stoddart, E. A. Weiss, M. R. Wasielewski, D. T. Co, J. Am. Chem. Soc. 2016, 138, 6163 – 6170.
[38] O. V. Dolomanov, L. J. Bourhis, R. J. Gildea, J. A. K. Howard, H. Puschmann, J. Appl. Crystallogr. 2009, 42, 339 – 341.
[39] G. Sheldrick, Acta Crystallogr. Sect. A 2008, 64, 112 – 122.
[40] G. Sheldrick, Acta Crystallogr. Sect. C 2015, 71, 3 – 8.
[41] B. Kaduk, T. Kowalczyk, T. Van Voorhis, Chem. Rev. 2012, 112, 321 – 370.